

# On-Chip Polarization Rotators

Zhi-Shan Hou, Xiao Xiong, Jia-Ji Cao, Qi-Dai Chen, Zhen-Nan Tian,\*  
Xi-Feng Ren,\* and Hong-Bo Sun\*

On-chip polarization manipulation is proposed via a waveguide that is adiabatically twisted along its longitudinal axis, which can be fundamental building blocks for polarization-encoded optical communication and information processing. With the help of femtosecond direct laser writing, the polarization rotators for both telecom and visible wavelengths are fabricated, which show polarization conversion efficiencies of >90% at 1550 nm and ≈80% at 646 nm, respectively. Furthermore, a polarization router consisting of multiple waveguides with different twisting angles is demonstrated. With the polarization router, photons with different polarizations are directed to different paths. Based on such platform, the path entanglement between the photons can be transformed to polarization entanglement, which will extend the quantum information technology to higher-dimensional Hilbert space.

## 1. Introduction

Photonic integrated circuits (PICs) with functional components enable information processing within one single chip.<sup>[1,2]</sup> Compared to conventional free-space optics, they are compact, scalable, stable to environment, and possess low power consumption. A vast spectrum of progress has been facilitated, including communication,<sup>[3–5]</sup> information processing,<sup>[6–8]</sup>

detection,<sup>[9,10]</sup> sensing,<sup>[11–14]</sup> and so on. Specifically, to process polarization-encoded information in PICs, controlling of the polarization states is necessary, which requires the combinations of polarization isolator, polarization rotator, polarizer retarder, and so on.<sup>[15–18]</sup> In free space, there are already many examples of implementing polarization manipulation.<sup>[19–21]</sup> Recently, metamaterials also allow polarization conversion with near-perfect conversion efficiency.<sup>[22,23]</sup> However, we focus on the on-chip polarization conversion using integrated waveguides. So far, the methods for manipulating the polarization states of photons in PICs can be roughly classified into three categories:

I) The most common one is to make the waveguide cross-section asymmetric, so that the horizontal and vertical polarization modes are no longer orthogonal and interfere with each other.<sup>[24,25]</sup> This type of devices requires high accuracy in fabrication and is usually sensitive to wavelength. II) The second one is based on the mode evolution, where the polarization of the photon changes as the waveguide geometry is slowly engineered. Since the waveguide cross sections usually vary in the vertical direction, this type of devices is difficult to fabricate with the top-down process.<sup>[26,27]</sup> III) The third type relies on surface plasmon polaritons, which are excited selectively by perpendicular polarization of photons.<sup>[28,29]</sup> In 2015, Zhu's group has demonstrated a plasmonic polarization generator that can reconfigure an input polarization to all types of polarization states simultaneously.<sup>[8]</sup> Although these plasmonic devices can be made very small (several micrometers), their performance is severely encumbered by the absorption of the metal.

For type-II polarization rotators, they have a lot of advantages. For example, their broad bandwidth benefits the operations involving pulsed lasers. And unlike the type-I ones, their requirement on fabrication accuracy is relaxed due to the nature of adiabatic mode evolution.<sup>[30,31]</sup> Although the top-down lithography techniques are restricted in their fabrication, people have developed many other techniques that can deal with 3D nanostructures, such as self-assembly and 3D printing.<sup>[32,33]</sup> Femtosecond direct laser writing (fs-DLW) is also one of them, which uses tightly focused ultrashort (fs scale) pulsed laser and changes the optical properties of materials via nonlinear multiphoton absorption.<sup>[34]</sup> Depending on the different materials and the applied laser power, the material properties may change because of polymerization, reduction, bond cleavage, phase change, and ablation.<sup>[35–38]</sup> Due to the small multiphoton absorption cross section and the short

Z.-S. Hou, J.-J. Cao, Prof. Q.-D. Chen, Dr. Z.-N. Tian, Prof. H.-B. Sun  
State Key Laboratory of Integrated Optoelectronics  
College of Electronic Science and Engineering  
Jilin University  
Changchun 130012, P. R. China  
E-mail: zhennan\_tian@jlu.edu.cn


Dr. X. Xiong, Prof. X.-F. Ren  
Key Laboratory of Quantum Information of CAS  
University of Science and Technology of China  
Hefei, Anhui 230026, P. R. China  
E-mail: renxf@ustc.edu.cn

Dr. X. Xiong, Prof. X.-F. Ren  
Synergetic Innovation Center of Quantum Information & Quantum  
Physics

University of Science and Technology of China  
Hefei, Anhui 230026, P. R. China

Prof. H.-B. Sun  
State Key Laboratory of Precision Measurement Technology and  
Instruments

Department of Precision Instrument  
Tsinghua University  
Haidian, Beijing 100084, P. R. China  
E-mail: hbsun@tsinghua.edu.cn

 The ORCID identification number(s) for the author(s) of this article can be found under <https://doi.org/10.1002/adom.201900129>.

DOI: 10.1002/adom.201900129

light–matter interaction time, fs-DLW has higher resolution and lower thermal damage. Besides, it provides higher designability of the composites and does not require high-vacuum or low-temperature condition.<sup>[39,40]</sup>

In this paper, we fabricate twisted waveguides with precisely controlled 3D feature using fs-DLW technique. Based on adiabatic mode evolution, the twisted waveguides enable conversion of incident light to its orthogonal polarization during its transmission. The on-chip polarization conversion efficiency is measured as >90% at 1550 nm and ≈80% at 646 nm, which are in good agreement with the finite-difference time-domain (FDTD) simulations. The polarization rotators maintain high conversion efficiency for a broad bandwidth (wavelength of 1400–1700 nm) without extra insertion loss (0.096 dB). More importantly, an arbitrary polarization state can be realized by simply choosing the twisting angle of waveguides. As a proof of concept, we demonstrate a polarization router using four waveguides with different twisting angles (0°, 30°, 60°, and 90°). The polarization conversion efficiencies of the four channels are all greater than 85%, showing the potential of twisted waveguides for polarization-encoded information processing.

## 2. Device Fabrication

The polarization rotator based on mode evolution is shown in **Figure 1**, which consists of the twisted part (blue) and input/output coupling parts (gray). The waveguide is made of SU-8 and sits on silica substrate. Details on the fabrication process are provided in the Supporting Information. We define the

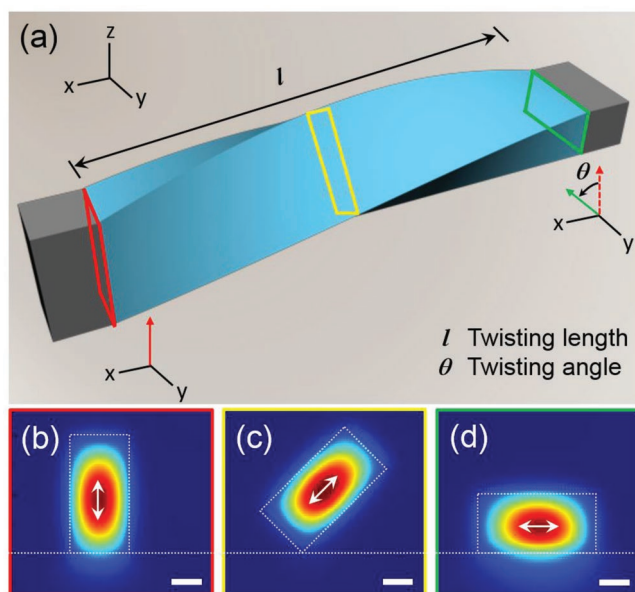


**Figure 1.** a) Schematic representation of the twisted waveguide based on adiabatic mode conversion. The hollow rectangles represent the cross sections at the input (red), middle (yellow), and output (green) of the polarization rotator. b–d) The simulated electric field distributions at the b) input, c) middle, and d) output of the twisted waveguide, with  $\theta = 90^\circ$  and  $l = 200 \mu\text{m}$ . White arrows in the center denote the polarization of the optical field. Scale bars: 1  $\mu\text{m}$ .

angle that output part is rotated with respect to the input part as twisting angle  $\theta$ , and the length of twisted part as twisting length  $l$ . In our experiments, the twisting length  $l$  ranges from 50 to 500  $\mu\text{m}$ . We also performed numerical simulations with Lumerical FDTD for a twisted waveguide with  $\theta = 90^\circ$  and  $l = 200 \mu\text{m}$ . At the input port, the waveguide has a cross section of  $2 \times 4 \mu\text{m}^2$  and supports the fundamental mode as shown in Figure 1b. This fundamental mode is polarized vertically, denoted as transverse-magnetic (TM) mode. As the TM mode propagates along the twisted waveguide, it gradually converts to transverse-electric (TE) mode as shown in Figure 1d. In the middle of propagation, the electric field distribution in twisted waveguide is displayed in Figure 1c, which remains as well-confined waveguide mode. These results show that the optical field maintains its alignment with the waveguide geometry during propagation, thus facilitating the polarization manipulation.<sup>[41]</sup> According to the adiabatic theorem, the twisted waveguide remains in its instantaneous eigenstate (the fundamental mode) if a given perturbation (the twisting) is acting on it slowly enough.<sup>[42]</sup> It implies that a longer waveguide with slower twisting is favorable, which is also the prerequisite for perfect polarization conversion.<sup>[43]</sup>

Now, we show some scanning electron microscope (SEM) images of different samples. **Figure 2a** shows the twisted waveguides, with  $\theta = 90^\circ$  and twisting length of 150, 100, and 50  $\mu\text{m}$ , respectively. For the waveguide with  $l = 150 \mu\text{m}$ , a  $90^\circ$  smooth rotation of the waveguide orientation is clearly shown in Figure 2b. The cross bars on top of the waveguides are markers to denote the cut-off of twisted part. Thanks to the high precision of fs-DLW processing, a waveguide with arbitrary twisting angle can be fabricated. In Figure 2c, we show several twisted segments with  $\theta = 30^\circ$ – $360^\circ$  with exaggerated size, just to showcase the arbitrary twisting angles. Experimentally, the samples that we measured are twisted much more slowly to fulfill adiabatic condition.

## 3. Polarization Rotators for Telecom and Visible light

For a twisted waveguide with  $\theta = 90^\circ$ , a TM input can be converted to TE output, as we have shown in Figure 1. This type of waveguide is also called polarization rotator. In the following, we will demonstrate the polarization rotators at both telecom and visible wavelengths.

The experimental setup to characterize the polarization rotators is displayed in **Figure 3a**. The laser ( $\lambda = 1550 \text{ nm}$  or 646 nm) is coupled into the sample with single-mode fiber (SMF). Before injected into the sample, the light is tuned as TM polarization by passing through the half-wave plate (HWP) and quarter-wave plate (QWP). The output from the sample is collected with lens and directed into two paths with polarization beam splitter (PBS). Two power meters (D1 and D2) are used to record the TE and TM components of waveguide output, respectively. Denoting the counts of D1 and D2 as  $P_{\text{TE}}$  and  $P_{\text{TM}}$ , we obtain the polarization conversion efficiency expressed as

$$\eta_{\text{TM} \rightarrow \text{TE}} = \frac{P_{\text{TE}}}{P_{\text{TM}} + P_{\text{TE}}} \quad (1)$$

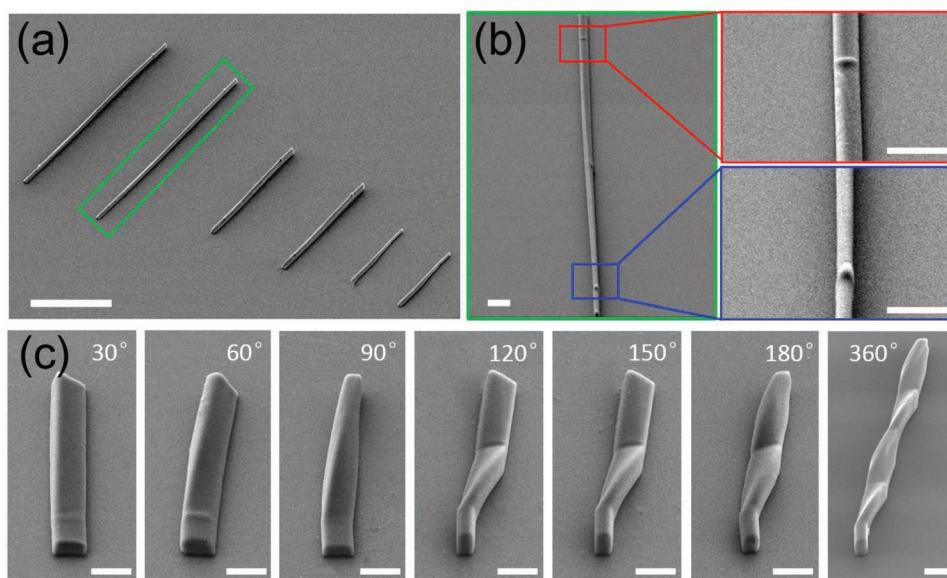


**Figure 2.** a) SEM image of the polarization rotators with twisting lengths of 150, 100, and 50  $\mu\text{m}$  (from left to right). Scale bar: 100  $\mu\text{m}$ . b) Enlarged view of the sample selected as green rectangle in panel (a) with twisting length of 150  $\mu\text{m}$ . Insets: zoom-in of the coupling parts. Scale bars: 10  $\mu\text{m}$ . c) SEM images of twisted segments with different twisting angles. Scale bars: 10  $\mu\text{m}$ .

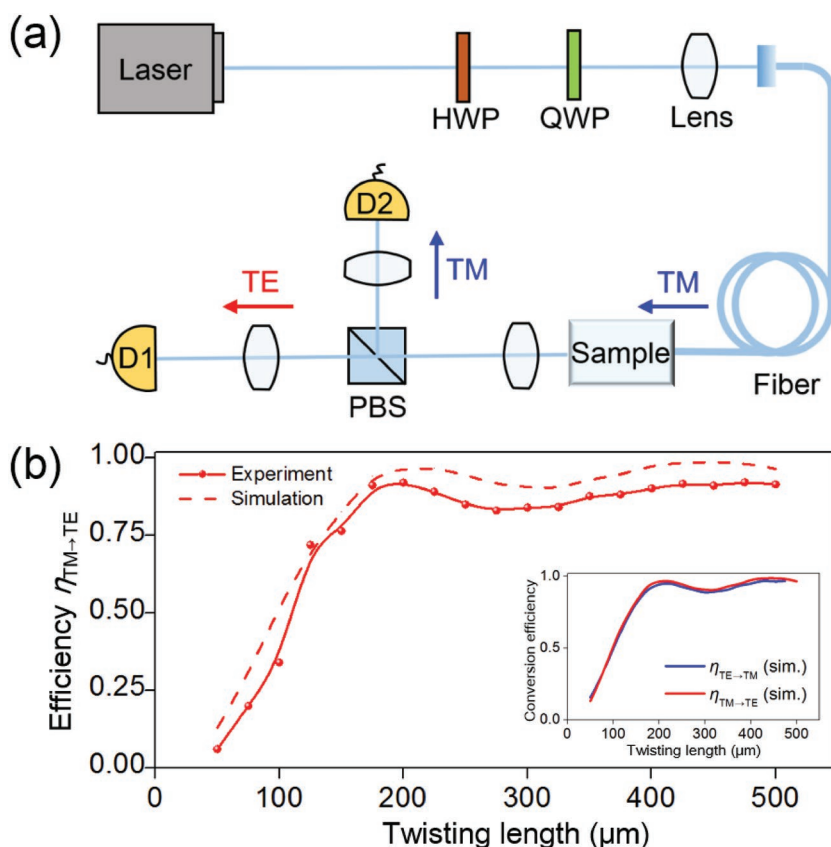


**Figure 3.** a) Experimental setup to measure the polarization rotators. HWP: half-wave plate; QWP: quarter-wave plate; PBS: polarization beam splitter; D: detector. b) The polarization conversion efficiency  $\eta_{\text{TM} \rightarrow \text{TE}}$  for polarization rotators at  $\lambda = 1550 \text{ nm}$  with different twisting length. Inset: The polarization conversion efficiency with either TM or TE polarization input from the same input port.

Before measuring our samples, we coupled SMF directly to the PBS and tuned the HWP and QWP to have zero count in D1, so that the injected light is purely TM polarized. To facilitate coupling, the coupling parts of all samples are 500  $\mu\text{m}$  in length, and we cleaved the samples to assure smooth end facets.<sup>[44]</sup>

The polarization conversion efficiency for polarization rotators with different twisting length is shown in Figure 3b. The efficiency  $\eta_{\text{TM} \rightarrow \text{TE}}$  increases as the twisting length increases from  $l = 50 \mu\text{m}$  to  $l = 170 \mu\text{m}$ . For  $l > 170 \mu\text{m}$ , the average efficiency maintains above 80%, with the maximum  $\eta_{\text{TM} \rightarrow \text{TE}} = 92.1\%$  at  $l = 200 \mu\text{m}$ . The efficiency for longer twisting length saturates, since the adiabatic condition has been satisfied. The trend of experimental results agrees well with the simulations. The small discrepancy between them may be due to the imperfect fabrications. As for the spectral response of the polarization rotator (see Supporting Information), it maintains high polarization conversion efficiency  $>84\%$  within the spectral range of 1400–1700 nm, which is favorable for pulse operation.

We also simulated the polarization conversion efficiency  $\eta_{\text{TE} \rightarrow \text{TM}}$  when TE polarization is injected from the same port (cross section of  $2 \times 4 \mu\text{m}^2$ ). The result is plotted in the inset of Figure 3b together with  $\eta_{\text{TM} \rightarrow \text{TE}}$ . As can be seen,  $\eta_{\text{TE} \rightarrow \text{TM}} \approx \eta_{\text{TM} \rightarrow \text{TE}}$ . It implies



that for any arbitrary input polarized at  $\phi$ , after passing through the polarization rotator ( $\theta = 90^\circ$ ), it exits as photons polarized at  $(\phi + 90^\circ)$ . Additionally, if the input is a left circular polarization TE +  $i$ TM, the output becomes TM +  $ie^{i\Delta\phi}$ TE; thus, a right circularly polarized light is readily achieved. Here, the phase difference  $\Delta\phi$  comes from the different wavevectors between the orthogonal polarization components and can be compensated by engineering the waveguide length.”

Besides, we characterized the propagation loss for straight waveguide with no twisting (see Supporting Information). A loss of 7.5 dB  $\text{cm}^{-1}$  is measured, which is a little high. This might originate from the nonuniform polymerization of SU-8 during laser exposure and can be further improved by optimizing the fabrication procedure. For example, a lower processing speed and better laser power might help. As for the insertion loss induced by the twisting, we measured a loss of 0.096 dB for polarization rotator with  $l = 500 \mu\text{m}$ , which is negligible. Similar to the polarization rotators at telecom wavelength, a polarization rotator at visible wavelength also plays an important role in information processing.<sup>[45,46]</sup> However, the reduction in wavelength means a reduction in the waveguide size as well, which imposes higher demands on the fabrication precision. So far, there is little study on the polarization rotator for visible light. Here, we extended our study to polarization devices at visible wavelength and demonstrated a polarization rotator at  $\lambda = 646 \text{ nm}$ . As shown in the inset of Figure 4, the device has a cross section of  $1 \times 2 \mu\text{m}^2$  on the left and  $2 \times 1 \mu\text{m}^2$  on the right. Similar to the case at telecom wavelength,  $\eta_{\text{TM} \rightarrow \text{TE}}$  increases at first and maintains an average value >80% for  $l > 125 \mu\text{m}$ . Experimentally, we measured both the conversion efficiency of  $\eta_{\text{TM} \rightarrow \text{TE}}$  and  $\eta_{\text{TE} \rightarrow \text{TM}}$ . Different from the previous  $\eta_{\text{TE} \rightarrow \text{TM}}$ , here we measured  $\eta_{\text{TE} \rightarrow \text{TM}}$  by using the cross section of  $2 \times 1 \mu\text{m}^2$  as the input port. The consistence of  $\eta_{\text{TE} \rightarrow \text{TM}}$  with  $\eta_{\text{TM} \rightarrow \text{TE}}$  proves the

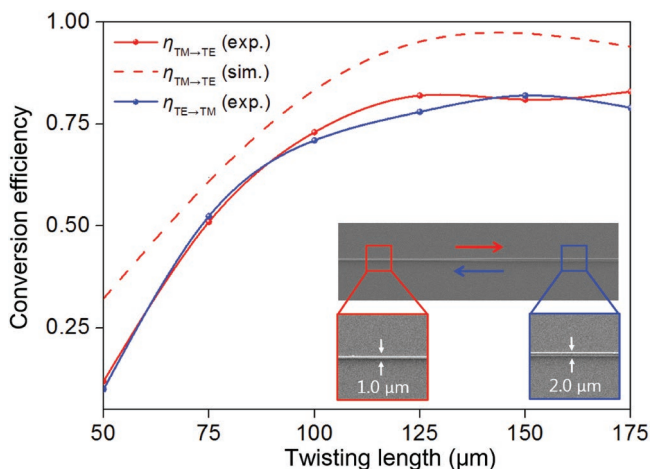


**Figure 4.** The polarization conversion efficiency for polarization rotators at  $\lambda = 646 \text{ nm}$  with different twisting length.  $\eta_{\text{TM} \rightarrow \text{TE}}$  is obtained when TM polarization is input from the port with cross section of  $1 \times 2 \mu\text{m}^2$ , while  $\eta_{\text{TE} \rightarrow \text{TM}}$  corresponds to TE polarization input from the port with cross section of  $2 \times 1 \mu\text{m}^2$ . Inset: the SEM images of polarization rotator at visible wavelength, indicated with the measuring conditions for  $\eta_{\text{TM} \rightarrow \text{TE}}$  (red) and  $\eta_{\text{TE} \rightarrow \text{TM}}$  (blue), respectively.

time-reversal symmetry of our device, which is also known as reciprocity.

Power  $P_m$  accumulated in mode  $m$  is<sup>[43]</sup>

$$P_m(z) = 2|b_\tau(0)|^2 \left| \frac{\tau}{\delta\beta} \right|^2 [1 - \cos(\delta\beta z)] \quad (2)$$

where mode  $\tau$  is the initially excited mode,  $\beta$  is the local propagation constant of mode  $m$ , and  $\delta\beta$  is the difference between the propagation constants of modes  $m$  and  $\tau$ . According to Equation (2), the power lost to mode  $m$  can be minimized by maximizing the ratio of  $\delta\beta$  to  $\tau$ , in effect allowing modes to dephase before substantial power exchange takes place. In our case, both modes  $m$  and  $\tau$  are in the same polarization, and we target to minimize/maximize the coupling into the same/orthogonal polarization. On one hand, use of a large aspect ratio waveguide ensures greatly differing rates of propagation. For example, in our experiment, a waveguide with cross section of  $2 \times 4 \mu\text{m}^2$  results in a large modal refractive index difference between TM and TE modes, which facilitates the dephasing between incident TM wave and converted TE wave. On the other hand, for an achievable  $\delta\beta$ , the ratio of  $\delta\beta$  to  $\tau$  can always be increased through a longer transition. This is because the coupling coefficient between modes  $m$  and  $\tau$  is proportional to the rate of change of the waveguide, and a longer transition corresponds to a lower change rate. As for the preparation of arbitrary polarization state, it is equivalent to the condition that controls the mode coupling, by tuning the twisting angle of the waveguides when transition length is fixed.

#### 4. Polarization Router

Similar to polarization rotator, polarization router is also one of the building blocks for polarization-encoded information processing. For a router, input signals are selectively routed to the target output ports with different modes through the predesigned architecture. Currently, most of the research on optical routers is encoded with wavelength. Few study reports on the polarization-encoded router, which directs the input signals into different paths with different polarization states. Having seen the good performance of twisted waveguide as polarization rotators, we designed a four-port polarization-encoded router based on four twisted waveguides. As an example, we selected the device working at telecom wavelength. In Figure 5a,b, the schematic representation of the polarization router and the SEM image of a showcase are displayed. It consists of one input port and four output ports, where the incident light is coupled into each output port through Y-shape coupler. And each output path includes the twisted part, with twisting angle  $\theta = 0^\circ, 30^\circ, 60^\circ,$  and  $90^\circ$ , respectively. The real samples that we measured are shown in Figure 5c, which have a cross section of  $2 \times 4 \mu\text{m}^2$  at the input port, and a twisted part of  $l = 500 \mu\text{m}$ . The zoom-in view of the Y-shape coupler is displayed in Figure 5d, showing a smooth transition from one waveguide to two waveguides.

We tested the performance of twisted waveguides with  $\theta = 0^\circ\text{--}180^\circ$  (see Supporting Information). Results show that, with input light polarized at  $\phi$ , after passing through a twisted

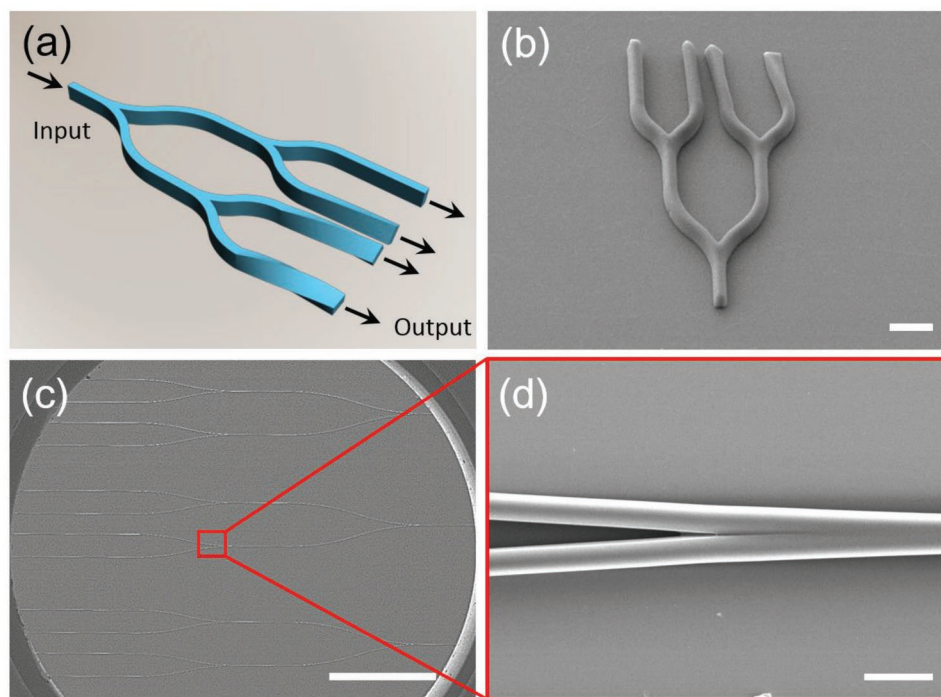


**Figure 5.** a) The schematic diagram of the polarization router. b) SEM image (at 45° view angle) of a showcase of the polarization router. Scale bar: 10 μm. c) SEM image of the polarization routers we experimentally measured, in which the twisting lengths are 500 μm. Scale bar: 1 mm. d) Zoom-in view of the beam splitting part. Scale bar: 10 μm.

waveguide with  $\theta$ , it exits as photons polarized at  $(\phi + \theta)$ . Specially, for a waveguide with  $\theta = 45^\circ$ , the out signal consists of 50/50 TE/TM components, regardless of an input of TE or TM polarization.

To characterize the polarization router, we modified the experimental setup in Figure 3a. We inserted a polarizer behind each output port of the router and used a set of lenses to capture the signals passing through polarizers. And each lens is followed by a charge coupled device (CCD) camera to record the output signals. We denote the different output ports with hollow rectangles as illustrated in Figure 6a. As shown in Figure 6b, at each port, as we rotated the inserted polarizers into different angles (illustrated by black arrows), the dark-field images of the output signals change. We extracted the gray values of output signals in dark-field images and plotted them for the corresponding output ports in Figure 6c. The gray values show sinusoidal dependence on the rotated angle of the inserted polarizer. When the inserted polarizer has the same orientation as the twisted part at each output port, the detected signal reaches its maximum, indicating a high rotation efficiency of the incident polarization. We do the normalization at each output port as:  $I_s + I_n = 1$ . Denote the output component that is polarized at the twisting angle  $\theta$  as signal  $I_s$  (maximum of the curve), and the other component that is orthogonal to  $\theta$  as noise  $I_n$  (minimum of the curve). We obtained the signal addressing efficiency  $\eta_{\text{TM} \rightarrow \theta}$  at each output port as

$$\eta_{\text{TM} \rightarrow \theta} = \frac{I_s - I_n}{I_s + I_n} \quad (3)$$

From Figure 6c, the efficiencies are extracted as  $\eta_{\text{TM} \rightarrow \theta} = 96.55\%$  (red), 91.94% (green), 85.72% (blue), and 86.51% (magenta), respectively. To further improve the efficiencies, increasing the twisting length  $l$  and reducing the roughness of the waveguide surface would help. Nevertheless, the high addressing efficiency proves that the polarization router is able to direct the input polarization into different polarizations. Note that, the data in Figure 6c are normalized so that  $I_s + I_n = 1$  at each output port. The four-port output light intensity ratio is 11.9: 25.11:42.8: 18.04.

## 5. Conclusion

In summary, we demonstrate a series of devices for on-chip polarization manipulation using fs-DLW. The polarization rotators for both telecom and visible wavelengths are fabricated, which show polarization conversion efficiencies of >90% at 1550 nm and ≈80% at 646 nm, respectively. Furthermore, a polarization router consisting of multiple twisted waveguides with different twisting angles is demonstrated. With the polarization router, photons with different polarizations can be directed to different paths. Because of the simple design, low insertion loss, and broad bandwidth, the on-chip polarization-encoded devices will surely find wide applications for compact, scalable, and high-dimensional information technology. We envision that the demonstrations in this article inspire more novel and functional designs of on-chip devices, as well as optimization on the current technique for a better platform.

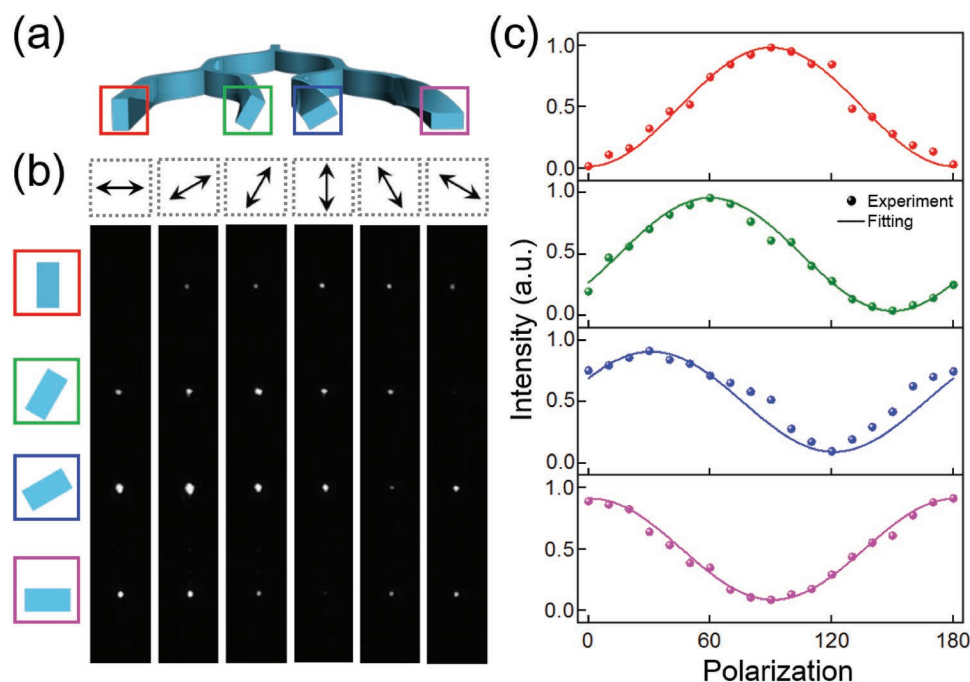


**Figure 6.** a) The schematic diagram of the polarization router with four output ports twisted by different angles:  $\theta = 0^\circ$  (red),  $\theta = 30^\circ$  (green),  $\theta = 60^\circ$  (blue), and  $\theta = 90^\circ$  (magenta). b) Dark-field images at the output ports, where the polarizers inserted behind each port are rotated at different angles (black arrows). From left to right, black arrows represent angles of  $0^\circ$ ,  $30^\circ$ ,  $60^\circ$ ,  $90^\circ$ ,  $120^\circ$ , and  $150^\circ$ , respectively. c) The normalized efficiency at each output port as a function of the rotated angle of polarizers.

## Supporting Information

Supporting Information is available from the Wiley Online Library or from the author.

## Acknowledgements

Z.-S.H. and X.X. contributed equally to this work. Support by the National Natural Science Foundation of China (NSFC) (61590930, 61805098, 61590932, 61825502, and 61435005), the Anhui Initiative in Quantum Information Technologies (AHY130300), the Strategic Priority Research Program of the Chinese Academy of Sciences (XDB24030601), the National Key R&D Program (2016YFA0301700), and the Fundamental Research Funds for the Central Universities is gratefully acknowledged.

## Conflict of Interest

The authors declare no conflict of interest.

## Keywords

femtosecond direct laser writing, microwaveguides, multiphoton absorption, polarization rotators, polarization router, twisted waveguides

Received: January 22, 2019  
Published online: March 6, 2019

- [1] S. Wang, D. Dai, *Opt. Lett.* **2018**, *43*, 2531.  
[2] S. M. Eaton, P. R. Herman, *Top. Appl. Phys.* **2012**, *123*, 155.  
[3] D. F. Welch, F. A. Kish, R. Nagarajan, C. H. Joyner, R. P. Schneider, V. G. Dominic, M. L. Mitchell, S. G. Grubb, T. K. Chiang, D. D. Perkins, A. C. Nilsson, *J. Lightwave Technol.* **2007**, *24*, 4674.

- [4] K. Wang, A. Nirmalathas, C. Lim, E. Wong, K. Alameh, H. Li, S. Skafidas, *Opt. Lett.* **2018**, *43*, 3132.  
[5] L. T. Feng, M. Zhang, Z. Y. Zhou, M. Li, X. Xiong, L. Yu, B. S. Shi, G. P. Guo, D. X. Dai, X. F. Ren, G. C. Guo, *Nat. Commun.* **2016**, *7*, 11985.  
[6] J. Mower, N. C. Harris, G. R. Steinbrecher, F. Najafi, Y. Lahini, T. Baehrjones, *Rev. Écon.* **2015**, *20*, 170.  
[7] J. Liu, S. M. Li, L. Z, A. D. Wang, S. Chen, C. Klitis, C. Du, Q. Mo, M. Sorel, S. Y. Yu, X. L. Cai, J. Wang, *Light: Sci. Appl.* **2018**, *7*, 17148.  
[8] L. Li, T. Li, X. M. Tang, S. M. Wang, Q. J. Wang, S. N. Zhu, *Light: Sci. Appl.* **2015**, *4*, e330.  
[9] V. Lien, K. Zhao, Y. Berdichevsky, Y. H. Lo, *IEEE J. Sel. Top. Quantum Electron.* **2005**, *11*, 827.  
[10] N. K. Fontaine, R. P. Scott, S. J. B. Yoo, *Opt. Commun.* **2011**, *284*, 3693.  
[11] C. J. Chung, X. Xu, Z. Pan, F. Mokhtari-Koushyar, R. Wang, H. Yan, H. Subbaraman, R. T. Chen, *J. Lightwave Technol.* **2018**, *36*, 1568.  
[12] Z. Wang, H. Yan, S. Chakravarty, H. Subbaraman, X. Xu, D. L. Fan, A. X. Wang, R. T. Chen, *Opt. Lett.* **2015**, *40*, 1563.  
[13] M. Haque, N. S. Zacharia, S. Ho, P. R. Herman, *Biomed. Opt. Express* **2013**, *4*, 1472.  
[14] D. Cristea, R. Muller, I. Pavelescu, *Proc. SPIE* **1999**, *3680*, 1141.  
[15] Z. Li, M. H. Kim, C. Wang, Z. Han, S. Shrestha, A. C. Overvig, M. Lu, A. Stein, A. M. Agrawal, M. Lončar, N. F. Yu, *Nat. Nanotechnol.* **2017**, *12*, 675.  
[16] H. Deng, D. O. Yevick, C. Brooks, P. E. Jessop, *J. Lightwave Technol.* **2005**, *23*, 432.  
[17] R. Iyer, A. D. Bristow, Z. Yang, J. S. Aitchison, H. M. V. Driel, J. E. Sipe, A. L. Smirl, in *Slow and Fast Light, Technical Digest*, Optical Society of America, Washington **2006**, paper TuC3.  
[18] M. Schumann, T. Bückmann, N. Gruhler, M. Wegener, W. Pernice, *Light: Sci. Appl.* **2014**, *3*, e175.  
[19] S. Avner, I. Abdulhalim, *Opt. Lett.* **2009**, *34*, 1801.

- [20] Y. Fuzi, R. Lizhen, S. A. Jewell, J. R. Sambles, *Opt. Express* **2007**, *15*, 4192.
- [21] Z. Zhuang, Y. J. Kim, J. S. Patel, *Appl. Phys. Lett.* **2000**, *76*, 3995.
- [22] R. H. Fan, Y. Zhou, X. P. Ren, R. W. Peng, S. C. Jiang, D. H. Xu, X. Xiong, X. R. Huang, M. Wang, *Adv. Mater.* **2015**, *27*, 1201.
- [23] N. K. Grady, J. E. Heyes, D. R. Chowdhury, Y. Zeng, M. T. Reiten, A. K. Azad, A. J. Taylor, D. A. Dalvit, H. T. Chen, *Science* **2013**, *340*, 1304.
- [24] D. O. Dzibrou, V. D. T. Jj, M. K. Smit, *Opt. Lett.* **2013**, *38*, 1061.
- [25] D. Dai, J. Wang, S. He, *Prog. Electromagn. Res.* **2013**, *143*, 773.
- [26] H. Zhang, S. Das, Y. Huang, C. Li, *Appl. Phys. Lett.* **2012**, *101*, 021105.
- [27] X. Xiong, C. L. Zou, X. F. Ren, G. C. Guo, *Opt. Express* **2013**, *21*, 17097.
- [28] J. N. Caspers, M. Z. Alam, M. Mo, *Opt. Lett.* **2012**, *37*, 4615.
- [29] Y. H. Ding, H. Y. Ou, C. Peucheret, *Opt. Lett.* **2013**, *38*, 1227.
- [30] Y. Shani, C. H. Henry, R. C. Kistler, R. F. Kazarinov, *IEEE J. Quantum Electron.* **1991**, *27*, 556.
- [31] R. B. Hooker, R. S. Fan, *J. Lightwave Technol.* **1999**, *17*, 466.
- [32] D. Vega, P. R. Brito-Parada, J. J. Cilliers, *Chem. Eng. J.* **2018**, *350*, 653.
- [33] G. Huang, Y. Mei, *Small* **2018**, *14*, 1703665.
- [34] X. Wang, A. Kuchmizhak, E. Brasselet, S. Juodkazis, *Appl. Phys. Lett.* **2017**, *110*, 1.
- [35] W. Xiong, Y. S. Zhou, X. N. He, Y. Gao, M. Mahjourisamani, L. Jiang, T. Baldacchini, Y. F. Lu, *Light: Sci. Appl.* **2012**, *1*, e6.
- [36] M. Malinauskas, A. Zukauskas, G. Bickaускаite, R. Gadonas, S. Juodkazis, *Opt. Express* **2010**, *18*, 10209.
- [37] L. Wang, Q. D. Chen, X. W. Cao, R. Buividas, X. W. Wang, S. Juodkazis, H. B. Sun, *Light: Sci. Appl.* **2017**, *6*, e17112.
- [38] X. Q. Liu, Q. D. Chen, K. M. Guan, Z. C. Ma, Y. H. Yu, K. Q. Li, Z. N. Tian, H. B. Sun, *Laser Photonics Rev.* **2017**, *11*, 1600115.
- [39] Y. L. Sun, W. F. Dong, L. G. Niu, T. Jjiang, D. X. Liu, L. Zhang, Y. S. Wang, D. P. Kim, Q. D. Chen, H. B. Sun, *Light: Sci. Appl.* **2014**, *3*, e129.
- [40] H. B. Jiang, Y. L. Zhang, Y. Liu, X. Y. Fu, Y. F. Li, Y. Q. Liu, C. H. Li, H. B. Sun, *Laser Photonics Rev.* **2016**, *10*, 441.
- [41] C. Li, D. Dai, *Laser Optoelectron. Prog.* **2017**, *54*, 050003.
- [42] B. A. Garetz, G. E. Hall, G. A. K. Wallace, *Appl. Phys. Lett.* **1977**, *31*, 387.
- [43] M. R. Watts, H. A. Haus, E. P. Ippen, *Opt. Lett.* **2005**, *30*, 138.
- [44] X. Q. Sun, C. M. Chen, F. Wang, J. Sun, *Opt. Appl.* **2010**, *40*, 737.
- [45] D. Floess, J. Y. Chin, A. Kawatani, D. Dregely, H. U. Habermeier, T. Weiss, H. Giessen, *Light: Sci. Appl.* **2015**, *4*, e284.
- [46] L. Fan, *Science* **2012**, *335*, 447.